Enhancement of Third-Order Optical Nonlinearities in 3-Dimensional Films of Dielectric Shell Capped Au Composite Nanoparticles

Yong Yang and Masayuki Nogami*

Department of Materials Science and Engineering, Nagoya Institute of Technology, Showa, Nagoya, 466-8555, Japan

Jianlin Shi and Hangrong Chen

State Key Laboratory of High Performance Ceramics and Superfine Microstructure, Shanghai Institute of Ceramics, Chinese Academy of Sciences, Shanghai 200050, PRC

Guohong Ma and Singhai Tang

Physics Department, National University of Singapore, Singapore, 119260

Received: September 14, 2004; In Final Form: December 6, 2004

The composite nanoparticles of Au-core capped by CdS shells of different thickness were prepared and assembled into densely packed 3-dimensional films by the layer-by-layer self-assembly (LBL) technique. These films exhibited the 3-dimensional structure of densely packed Au@CdS composite nanoparticles and the shell thickness was tunable by changing the concentration of Cd^{2+}−thiourea complexes. These multilayer films exhibited enhanced third-order optical nonlinear responses and ultrafast response times (several picoseconds). The third-order nonlinear optical susceptibility of the film with the CdS shell thickness of 4.4 nm was estimated to be 1.48×10^{-9} esu and the value decreases with the increase of the CdS shell thickness. The enhancement of the optical nonlinearity was explained based on the calculation according to the electrostatic approximation by the solution of Laplace's equation under the boundary conditions appropriate to the model of core−shell nanoparticles, and mainly attributed to localized electric field effects in the CdS shell region. Additionally, the nonlinearity was optimized by determination of the values of the dielectric constant and thickness of the different shell.

Introduction

Nanoscale architectures of composite nanoparticles have attracted tremendous interest because of their potential applications in nanoelectronics devices, catalysis, molecular recognition, and nonlinear optical devices.[1,2] Especially, these composite nanoparticles with core−shell structure (CSNs) often exhibit improved physical and chemical properties over their single-component counterparts, making them attractive from both scientific and technological viewpoints.[3] Those CSNs can simultaneously provide scaffolds for devices and serve as building blocks for the creation of extended two- and three-dimensional ordered arrays.[4] The self-assembly of CSNs into super-structure, thin films, or 3D "artificial solids" offers an exciting pathway for the construction of materials with designer-specified optical, electrical, and catalytic properties.[5,6] Xia et al.[7] have prepared $Au@SiO_2$ core−shell colloids (with average diameter of hundreds of nanometers) with long-range ordered arrangement and explored the potential use of these core−shell colloids as building blocks to fabricate functional optical devices such as photonic crystals and plasmonic waveguides. Liz-Marzán et al.[8] have synthesized fcc (face centered cubic) opals with a suitable lattice constant to yield photonic band gap effects in the visible waveband based on silica-coated gold particles and studied their optical properties through transmission and specular reflectance measurements. Moreover, the metal−semiconductor core−shell composite nanoparticles could exhibit strongly enhanced nonlinear response by several orders of magnitude higher than their single-component based on the theoretical calculations[9] by Neeves et al. and related reports.[10] However, the optical nonlinear properties of these core−shell nanoparticles or films are seldom reported.

Materials with large third-order optical nonlinearity and ultrafast response time are essential for light-controlled phase and refractive index modulation for future applications in various fields such as optical telecommunications, optical data storage, optical computing, and information processing.[11] It is well-known that metal nanocrystallites embedded in transparent matrix exhibit unique linear and nonlinear optical properties due to local field enhancement near the surface plasmon resonance (SPR) of the metal. The metal particles' shape, dielectric environment, and structure are probably the most important parameters determining the surface plasmon frequency and the optical nonlinear properties.[12] A significant challenge for enhancing the optical nonlinear response in materials is controlling the structure of metal nanoparticles and achieving a high particle filling factor in the process of fabricating particles into host matrixes. In a previous paper,[13] we reported the preparation of sulfide semiconductor capped gold composite nanoparticles and fabricated these composite nanoparticles into $BaTiO_3$ thin films. However, the volume fraction of gold nanoparticles was very low because the excess gold−sulfide composite colloids were easy to precipitate in $BaTiO_3$ precursor solutions. Here, we applied a simple route based on the LBL method to self-assemble the densely packed 3-dimensional arrays of homoge-

* Address correspondence to this author. E-mail: nogami@mse.nitech.ac.jp.

10.1021/jp045854a CCC: $30.25
Published on Web 02/25/2005

SCHEME 1: Fabrication of 3-Dimensional Au@CdS Arrays

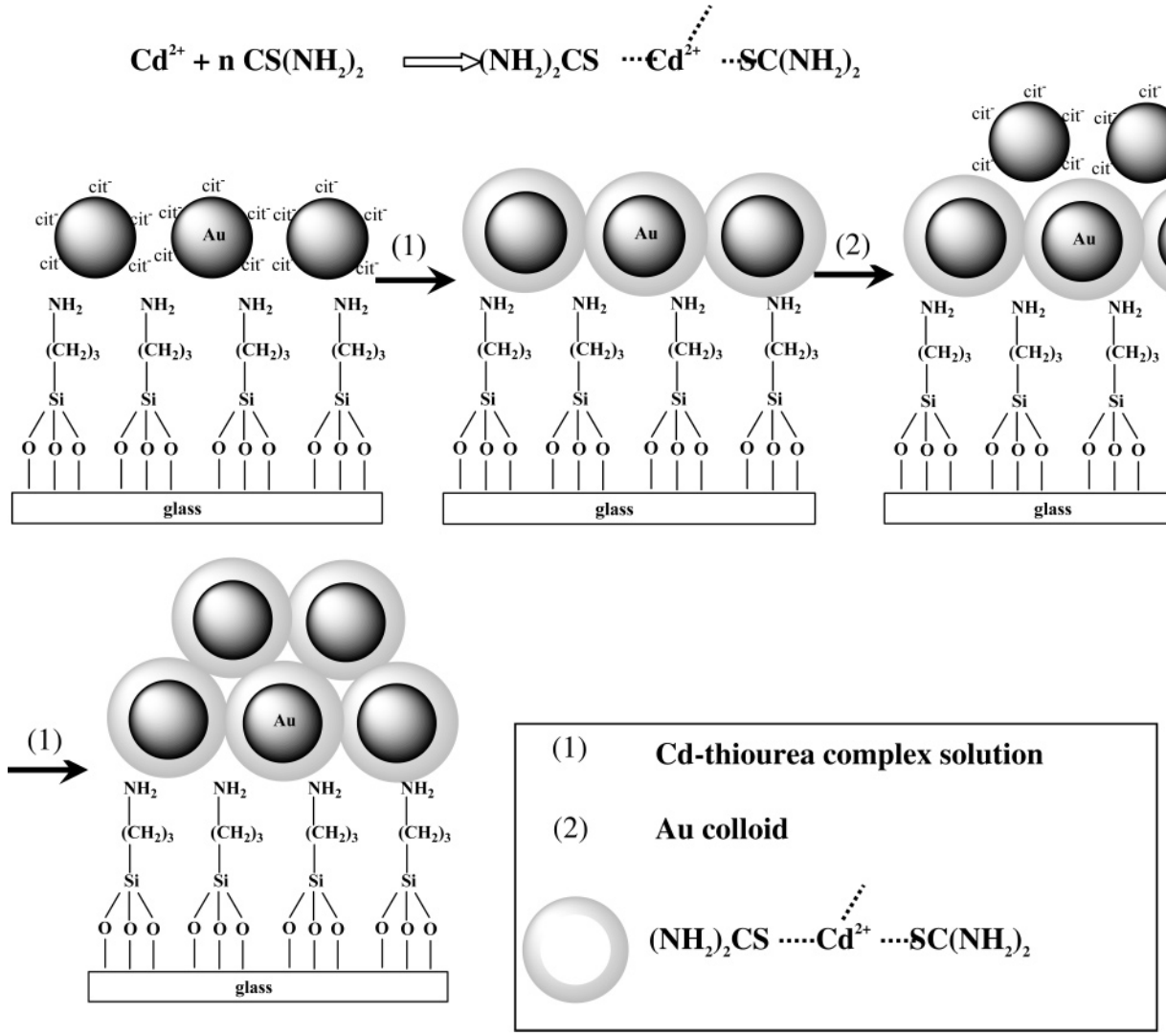

neous CdS coated gold nanoparticles. The method applied amine terminal groups in Cd^{2+}−thiourea complexes as a bifunctional cross-linker, to couple gold nanoparticles and fabricate into 3D arrays. The thickness of the CdS shell can be tuned by changing the concentration of Cd^{2+}−thiourea complexes. The volume fraction of gold nanoparticles was greatly increased due to the densely packed 3-dimensional structure. And the greatly enhanced optical nonlinear responses of these arrays were reported. Furthermore, the array of SiO_2 coated gold nanoparticles was also prepared in order to compare the dielectric effect of different shells. The enhancement mechanism of nonlinearity was also investigated according to the electrostatic approximation by the solution of Laplace's equation under the boundary conditions appropriate to the model of core−shell nanoparticles, and mainly attributed to localized electric field effects in the CdS shell region. Additionally, the nonlinearity was optimized by determination of the values of the dielectric constant and thickness of the different shell. The present paper also provides experimental evidence for Neeve's theory[9] about core−shell structures for the enhancement of nonlinear-optical susceptibility.

Experimental Section

A. Sample Fabrication. Gold colloids were prepared by the method of citrate reduction. In the process of thermal reduction, a gold sol was prepared by adding 1 mL of a 1 wt % of $HAuCl_4$ aqueous solution and 2 mL 38.8 mM sodium citrate aqueous solution into 90 mL of boiling water. The citrate ion acted as both a reductant and a stabilizer. After the solution had turned purple red within 30 s, it was cooled quickly in the ice bath. This resulted in a stable dispersion of gold particles with an average diameter of around 13.2 nm and 10% polydispersity.[14]

CdS colloids (25 mM) were prepared with $Cd(CH_3COO)_2$ and $CS(NH_2)_2$, $Cd(CH_3COO)_2 \cdot 2H_2O$ (1.0 mmol) was dissolved in acetic acid (20 mL), and 3.0 mmol of $CS(NH_2)_2$ was dissolved in 2-methoxyethanol (20 mL). Then two solutions were mixed and stirred for 60 min at 40 °C at an appropriate pH value. As prepared 25 mM CdS colloids were diluted by 2-methoxyethanol into 15 and 5 mM CdS colloids, respectively.Layer-by-layer self-assembled Au@CdS films were deposited on glass slides according to the following procedure. The specially cleaned glass slides[15] were placed in a dilute solution of 3-aminopropyltrimethoxysilane (APTMS) (4 g of APTMS in 36 g of CH_3OH) for 12 h and rinsed with copious amounts of CH_3OH upon removal. The APTMS-coated slides were subsequently immersed in colloidal gold solution for 12 h for assembling gold monolayer, followed by extensive rinsing with water. The Au@CdS monolayer was prepared from gold monolayer by treatment with CdS colloid solutions, and the Au@CdS multilayer films were prepared by repeating this process. The designed CdS shell thickness was obtained by dipping the gold

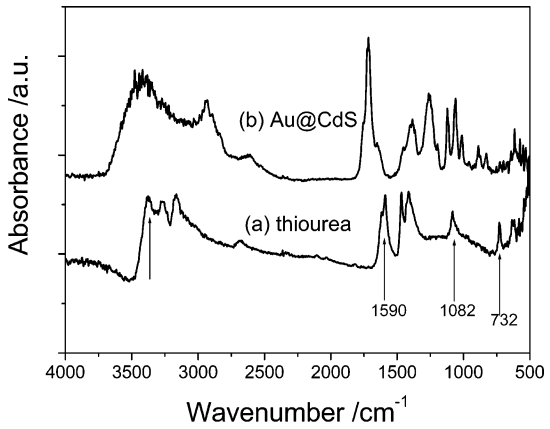

Figure 1. The FT-IR spectra of (a) pure thiourea and (b) Au@CdS powder precursors.

monolayer in CdS colloids of different concentrations. Au@SiO_2 multilayer films were also prepared with the above procedure, while the CdS colloids solutions were replaced by hydrolyzed APTMS 1:3:3 solution (APTMS:CH_3OH:0.15 M HCl = 1:3:3 mol %, sonicated for 2 h) for 12 h. Finally, these films were heat treated at 400 °C for 40 min in N_2 atmosphere in order to remove some organic agents.

B. Structural and Optical Characterization of Nanoparticle Films. FT-IR spectra of thiourea, un-annealed Au@CdS composite nanoparticle films were recorded with a FT-IR spectrometer (Jasco 460) in the wavenumber range of 400−4000 cm^{-1} on as-pressed disks using KBr as the binding materials. The surface morphologies of these films were examined with the dynamic force mode of an atomic force microscope (Seiko II, SPA-300HV). The microstructure and morphology of Au@CdS composite nanoparticles were measured with a JEOL JEM-2000EXII Transmission electron microscopy (TEM) operated at 200 kV. The absorption spectra of the Au@CdS films were recorded using a Jasco Ubest 570 UV−vis spectrophotometer. All the spectra were recorded in air at room temperature. The third-order nonlinear susceptibilities $\chi^{(3)}$ of the composite films were measured in accordance with OKE (Optical Kerr effect) technique[16] at room temperature. OKE experiments were performed by using a mode-locked Ti:sapphire femtosecond laser (Spectra-Physics Tsunami) with a pulse duration of 200 fs, repetition rate of 82 MHz, and a center wavelength of 800 nm. Bulk CdS polycrystals were used as standard samples.

Results and Discussion

The formation and reaction process of Au@CdS composite nanoparticles were investigated by FT-IR spectra. Figure 1 shows FT-IR spectra of thiourea and Au@CdS composite nanoparticles. In Figure 1a, these peaks at 3376, 3272, 3164 cm^{-1} (N−H stretching modes), 1590 cm^{-1} (−NH_2 bending modes), 1471 cm^{-1} (N−C−N stretching modes), 1415, 1082 cm^{-1} (NH_2 rocking vibration and N−C−N and C═S stretching vibrations), and 732 cm^{-1} (C═S stretching modes) showed a typical FT-IR spectra of pure thiourea. While the changes of those peaks in FT-IR spectra of Au@CdS precursors (Figure 1b), related to those of pure thiourea powder, indicate the formation of Au@CdS composite colloids. Those new peaks appearing at 3471 cm^{-1} (water), 2937 cm^{-1} (OH), 1712 cm^{-1} (C═O), 1253, 1058, 1003 cm^{-1} (C−O), and 887 cm^{-1} (OH) result from the solvent. Those peaks appearing at 3370, 1412 and 1115, 720, and 622 cm^{-1} correspond to the −NH_2, NH_2 rocking vibration and N−C−N and C═S stretching vibrations, un-coordinating C═S bond, and coordinating C═S bond, respectively. Compared with the FT-IR spectra of thiourea, the peak at 1115 cm^{-1} shifted from 1083 cm^{-1} can be attributed to the change in the nature of the N−C bond as well as of the C═S bond on coordination of thiourea through the sulfur atom; and the weakened peak at 720 cm^{-1} and the enhanced peak 622 cm^{-1} partially imply the reduction of double bond character of the C═S bond. All these indicate the formation of the Cd^{2+}−thiourea complexes:[17]

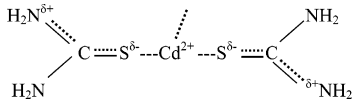

while those peaks at 3164 and 1590 cm^{-1} are weakened or disappear, which implies the Cd^{2+}−thiourea complexes are constructed on gold colloids through the NH_2^+ group.[18]

The packing structure and topography of 3-dimensional Au@CdS and Au@SiO_2 nanoparticles films were investigated by AFM and TEM. Those films exhibit densely packed spherical nanoparticles, as shown in Figure 2. It can be seen that the surfaces of glass substrates (Figure 2a−c) are completely covered by close packed Au@CdS composite nanoparticles, not by randomly distributed discrete particle islands and a number of vacant patches. Obviously, those close packed particles can provide a great building base for the next self-assembling composite nanoparticles.[18] These Au@CdS composite nanoparticles are uniform, and their average radii (removing the AFM tip−sample convolution) are around 11.0 (Figure 2a), 13.2 (Figure 2b), and 17.0 nm (Figure 2c) for those samples dipped in 5, 15, and 25 mM CdS colloids, respectively. The volume fraction (p) of gold particles was estimated to be 12.3%, 7.11%, and 3.16%, which are higher than that (0.2%) in Au@CdS/$BaTiO_3$ films.[13] It is evident that the 3D arrays of densely packed composite nanoparticles are helpful to increase the volume fraction of gold nanoparticles, and would enhance the third-order nonlinear optical response.[19] For the sample of Au@SiO_2 arrays (Figure 2d), these composite particles on the surface layer also exhibit fairly close packing structure and the radius of Au@SiO_2 composite nanoparticles is around 17 nm.

The TEM image of Au@CdS shown in Figure 3 clearly displays the typical core−shell structure of Au@CdS composite nanoparticles. These gold nanoparticles, with a diameter of 13.2 nm, are completely coated with CdS shell with a thickness of around 6 nm. The radius of the total composite nanoparticle is about 13 nm, which is consistent with the AFM analytical result (Figure 2b). The selected area electron diffraction (SAED) pattern of composite nanoparticle marked by a arrow shows polycrystalline diffraction rings, which include two sets of space lattice of Au fcc and CdS cubic zinc blende structure. The diffraction spots/rings are indexed to the CdS (200), Au (111), and CdS (220) or Au (200), Au (220), and CdS (420) planes, respectively.

Figure 4 shows the UV−vis absorption optical spectra of the Au@CdS composite films with different thicknesses of CdS shell. These curves exhibit exciton shoulders[20] around 440 nm and have onsets[21] in the 480−500 nm wavelength range, which are attributed to absorption edges of CdS nanocrystals. These absorption peaks at about 560 nm are attributed to the surface plasma resonance (SPR) of gold nanoparticles. It is interesting to note that the SPR peak is red-shifted with the increase of the thickness of the CdS shell. This red-shift was also consistent with the theoretical analysis result by Neeves[6] that the SPR peak would be red-shifted as the thickness of the shell was increased for the dielectric constants $\epsilon_{CdS} > \epsilon_{matrix}$ ($\epsilon_{CdS} = 5.4$).

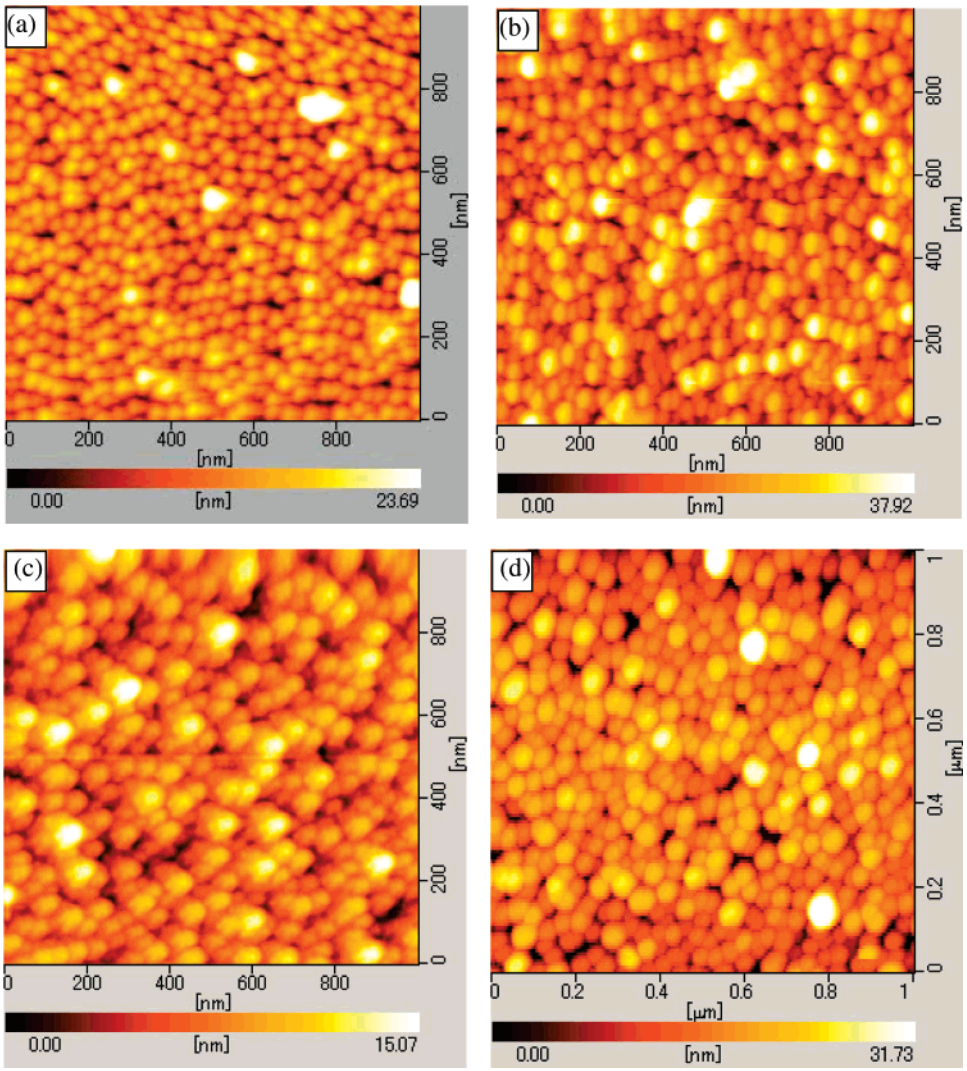

Figure 2. AFM images of Au@CdS films prepared with the different concentrations of Cd^{2+}−thiourea complexes (a) 5, (b) 15, and (c) 25 mM and (d) Au@SiO_2 film.

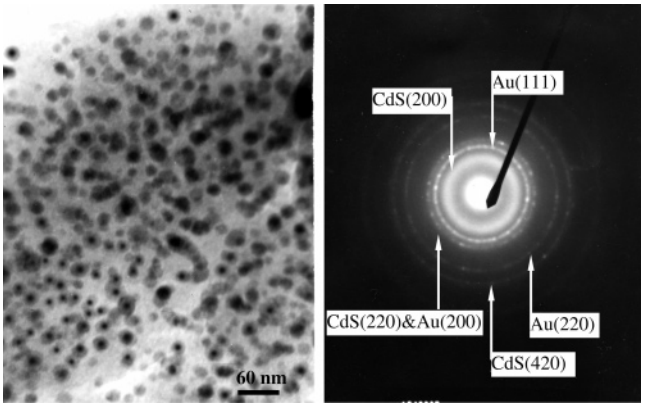

Figure 3. TEM images of Au@CdS film; the inset is the electron diffraction pattern of Au@CdS composite particles.

In this experiment, the third-order nonlinear susceptibilities $\chi^{(3)}$ of composite films were estimated at 800 nm by the time-resolved optical Kerr effect technique using a laser with a pulse width of 200 fs. The OKE signal originates from the third-order nonlinear optical effect due to the photoinduced change of refractive index, and the signal is proportional to the square of the third-order nonlinear susceptibility of the materials. Thus, the large OKE signal reflects that the composite has a large third-order nonlinear susceptibility. The third-order nonlinear

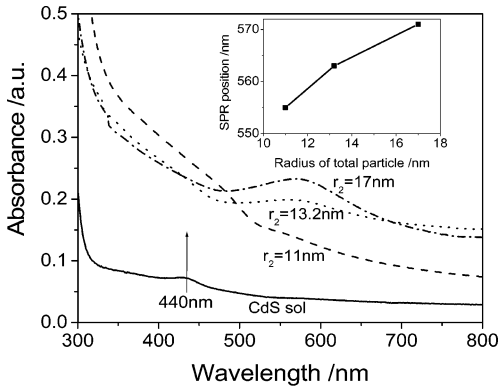

Figure 4. UV−vis absorbance spectra of Au@CdS films annealed at 400 °C. The inset shows the changes of SPR position with the different total particle radius (r_2).

susceptibility $\chi^{(3)}$(model) of thin films can be estimated with the following equation:[22]

$$\chi^{(3)} = \left[\frac{I_s}{I_{ref}}\right]^{1/2}\left[\frac{n_s}{n_{ref}}\right]^2\left[\frac{L_{ref}}{L_s}\right]\frac{1}{R}\chi_{ref}^{(3)} \qquad (1)$$

where n is the linear refractive index, I is the OKE signal intensity, L is the interaction distance of the pump light and

TABLE 1: The Total Particle Radii, Au-Core Radii, Au Volume Fraction, and $\chi^{(3)}$ Values of Samples and Referenced Results

properties	total radius/ nm	radius of Au-core/ nm	Au vol fraction/ %	$\chi^{(3)}$ value/esu
Au@CdS array	11.0	6.6	12.3	$(14.8 \pm 0.8) \times 10^{-10}$
Au@CdS array	13.2	6.6	7.11	$(9.8 \pm 0.8) \times 10^{-10}$
Au@CdS array	16.8	6.6	3.16	$(8.2 \pm 0.9) \times 10^{-10}$
Au@SiO_2 array	17.1	6.6	3.33	$(2.5 \pm 0.2) \times 10^{-11}$
Au@CdS/$BaTiO_3$[13]	4	2	0.2	$(7.2 \pm 1.4) \times 10^{-11}$
Au/SiO_2 film[25]		6	3.4	0.9×10^{-11}

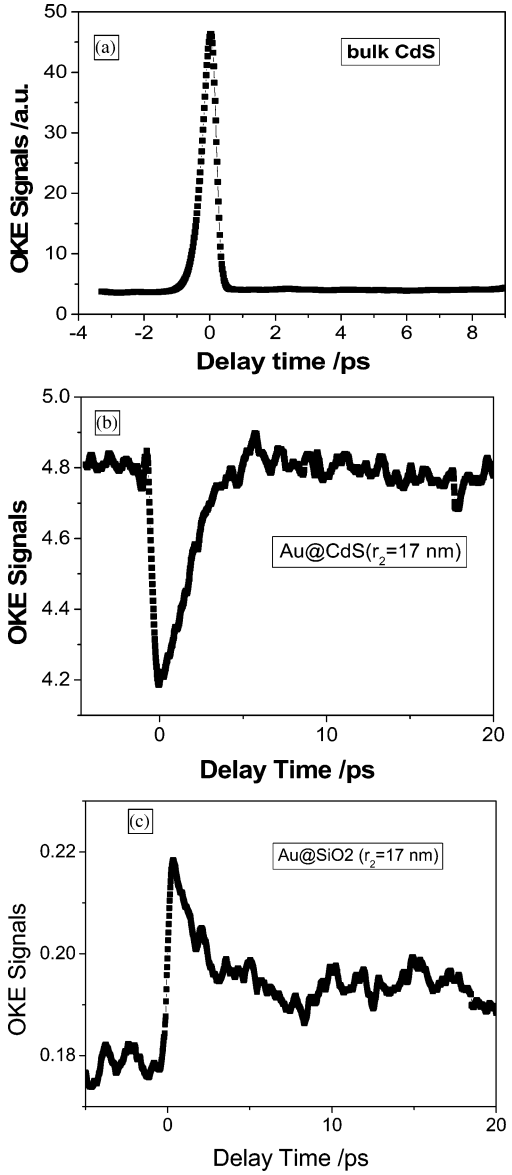

Figure 5. Femtosecond OKE spectra of bulk CdS, Au@CdS, and Au@SiO_2 films.

the probe light in the sample, R is the correction coefficient, and subscripts s and ref stand for sample and reference, respectively. The standard reference is bulk CdS and its $\chi^{(3)}$ is taken to be 2.4×10^{-12} esu at 780 nm.[23] The relative parameters and calculated $\chi^{(3)}$ values (model) of films are shown in Table 1.

All the OKE measurements were carried out at room temperature. Figure 5 shows the OKE signals of bulk CdS, Au@CdS, and Au@SiO_2 films. All these films exhibit ultrafast nonlinear response, with the decay time of about several picoseconds. The calculated $\chi^{(3)}$ values of Au@SiO_2 and

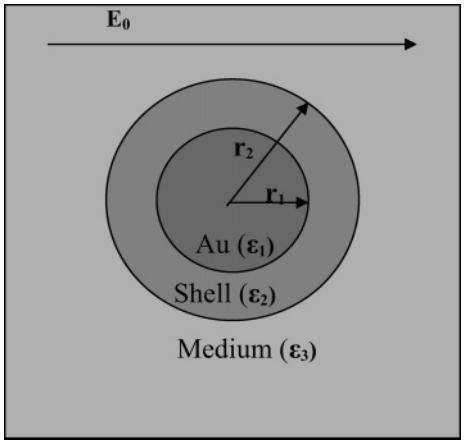

Figure 6. Simplified electromagnetic field scheme of a composite nanoparticle with core−shell structure.

Au@CdS films (total radius of 17 nm) are $(2.5 \pm 0.2) \times 10^{-11}$ and $(8.2 \pm 0.9) \times 10^{-10}$ esu, respectively. As we know, the $\chi^{(3)}$ value is dependent on the metal volume fraction, particle size, laser pulse width, and wavelength.[24] Ma et al.[25] reported a $\chi^{(3)}$ value of about 0.9×10^{-11} esu for the Au/SiO_2 film with a gold diameter of 12 nm and a Au volume fraction of 3.4% measured at 800 nm with a 200 fs pulse. The $\chi^{(3)}$ value of our Au@SiO_2 film is several times larger than the value reported by Ma at the same metal volume fraction, which indicates the optical nonlinearity is enhanced in the arrays of Au@SiO_2 core−shell nanoparticles. The enhancement of the third-order nonlinear susceptibility $\chi^{(3)}$ of the film should be attributed to the local-field enhancement.[9] The local field could be concentrated in both the core and shell regions of the CSNs at the surface-mediated plasma resonance, and this increased field is then utilized for self-enhancements of the optical nonlinearity from each component of the composite nanoparticles including Au-core and shell.[9] Furthermore, the $\chi^{(3)}$ value of the Au@CdS film is 30 times larger than that of the Au@SiO_2 film with the same shell thickness, and the enhancement is due to a higher refractive index and larger third-order nonlinear susceptibility of the CdS shell. The $\chi^{(3)}$ value of Au@CdS films increases with the decrease of thickness of the CdS shell.

To get a full understanding of the enhancement mechanism, the electric-field distribution in these arrays with core−shell structure is calculated and fitted according to the electrostatic approximation by the solution of Laplace's equation under the boundary conditions appropriate to the model of core−shell nanoparticles.[9] The simplified diagram of one core−shell composite nanoparticle subjected to an electromagnetic field is shown in Figure 6. The radii of the spherical Au-core and the total composite nanoparticle are r_1 and r_2, respectively. The dielectric permittivities of the core and the shell are ϵ_1 and ϵ_2, respectively. The fields $\boldsymbol{E}_1$ and $\boldsymbol{E}_2$ are the position-dependent complex vector fields in the core and shell, respectively, and $\boldsymbol{E}_0$ is the field far from the particle. The electric fields in the core and shell region are given by

$$\boldsymbol{E}_1 = \frac{9\epsilon_2\epsilon_3}{\epsilon_2\epsilon_a + 2\epsilon_3\epsilon_b}\boldsymbol{E}_0 \cos(\theta)\hat{e}_r - \frac{9\epsilon_2\epsilon_3}{\epsilon_2\epsilon_a + 2\epsilon_3\epsilon_b}\boldsymbol{E}_0 \sin(\theta)\hat{e}_\theta \tag{2a}$$

and

$$\boldsymbol{E}_2 = \frac{3\epsilon_3}{\epsilon_2\epsilon_a + 2\epsilon_3\epsilon_b}[(\epsilon_1 + \epsilon_2) + 2(\epsilon_1 - \epsilon_2)(r_1/r)^3]\boldsymbol{E}_0 \cos(\theta)\hat{e}_r - \frac{3\epsilon_3}{\epsilon_2\epsilon_a + 2\epsilon_3\epsilon_b}[(\epsilon_1 + \epsilon_2) - (\epsilon_1 - \epsilon_2)(r_1/r)^3]\boldsymbol{E}_0 \sin(\theta)\hat{e}_\theta \quad (2b)$$

where

$$\epsilon_a \equiv \epsilon_1(3 - 2P) + 2\epsilon_2 P \quad (3a)$$

$$\epsilon_b \equiv \epsilon_1 P + \epsilon_2(3 - P) \quad (3b)$$

$$P \equiv 1 - (r_1/r_2)^3 \quad (3c)$$

The factor P is the ratio of shell volume to total particle volume (V). Assuming that the nonlinear susceptibility of the shell $\chi_s^{(3)}$ is constant and the metal particles have the nonlinear susceptibility $\chi_m^{(3)}$, the effective third-order nonlinear susceptibility of composites $\chi_{eff}^{(3)}$ can be calculated by[26]

$$\chi_{eff}^{(3)}(\omega) = \chi_m^{(3)}(\omega)\frac{\int_{core}|\boldsymbol{E}_1|^2\boldsymbol{E}_1^2\,dV}{V|\boldsymbol{E}_0|^2\boldsymbol{E}_0^2} + \chi_s^{(3)}(\omega)\frac{\int_{shell}|\boldsymbol{E}_2|^2\boldsymbol{E}_2^2\,dV}{V|\boldsymbol{E}_0|^2\boldsymbol{E}_0^2} \quad (4)$$

where the nonlinear contribution of the host matrix (air) is negligible.

The electric-field magnitude ratios $\boldsymbol{E}_1/\boldsymbol{E}_0$ in the core region and $\boldsymbol{E}_2/\boldsymbol{E}_0$ in the interface region are calculated for Au@CdS and Au@SiO_2 composite nanoparticles using the above equations. The electric-field magnitude ratios of monodisperse Au particles (diameter of 13.2 nm) in SiO_2 film and CdS film are also calculated in order to compare the enhancement effectiveness of the core−shell structure. Only the gold permittivity is considered as a complex function of the incident field frequency ω in the calculations. The complex dielectric constant of the gold nanoparticle with a diameter of 13.2 nm is calculated by the method described in the literature.[9,27] The resonant behavior of the calculated electric field $\boldsymbol{E}_1/\boldsymbol{E}_2$ in the core-region and $\boldsymbol{E}_2/\boldsymbol{E}_0$ in the interface region is shown in Figure 7. It is clear from Figure 7a that the great enhancement of local electric field can be obtained in the core and interface when the SPR position is satisfied, and the enhancement decreases at the wavelength far from the SPR position. At 800 nm, the electric fields in the core and interface region of the core−shell structure are both stronger than those of gold particles dispersed in films, whether the matrix is CdS or SiO_2 (Figure 7b). It is obvious that the effective third-order nonlinear susceptibility of composite nanoparticles can become enhanced by the core−shell structure. Figure 8 is the spatial distribution of the electric field ratios in Au@SiO_2 and Au@CdS films at 800 nm, functioned as the radial distance from the core center. Although the amplitude of the electric field in the Au-core region is less than $\boldsymbol{E}_0$, the amplitude of the electric field in the CdS shell is substantially enhanced compared to the field far from the particle $\boldsymbol{E}_0$ at 800 nm, which is dominant for the enhancement of the effective optical nonlinearities in our samples. Especially, the electric fields in the core and shell region of Au@CdS nanoparticles get stronger enhancements compared with those of the Au@SiO_2 nanoparticle because CdS has a higher refractive index than SiO_2, and the nonlinear susceptibility of the CdS shell is also

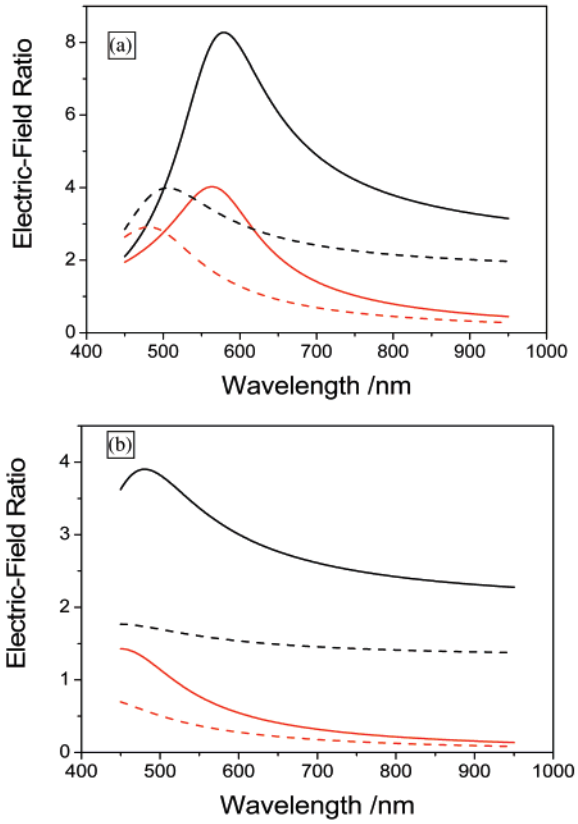

Figure 7. (a) Calculated magnitude of the electric-field ratio $\boldsymbol{E}_1/\boldsymbol{E}_0$ (red lines) in the core region and $\boldsymbol{E}_2/\boldsymbol{E}_0$ (black lines) in the interface region as a function of wavelength: solid line, Au@CdS film with the total radius of composite nanoparticles $r_2 = 17.0$ nm; dotted line, Au/CdS film. (b) Calculated magnitude of the electric-field ratio $\boldsymbol{E}_1/\boldsymbol{E}_0$ (red lines) in the core-region and $\boldsymbol{E}_2/\boldsymbol{E}_0$ (black lines) in the interface region: solid line, Au@SiO_2 film with the total radius $r_2 = 17.0$ nm; dotted line, Au/SiO_2 film. The dielectric constant of the SiO_2 shell is taken to be $\epsilon_2/\epsilon_0 = 2.3$.

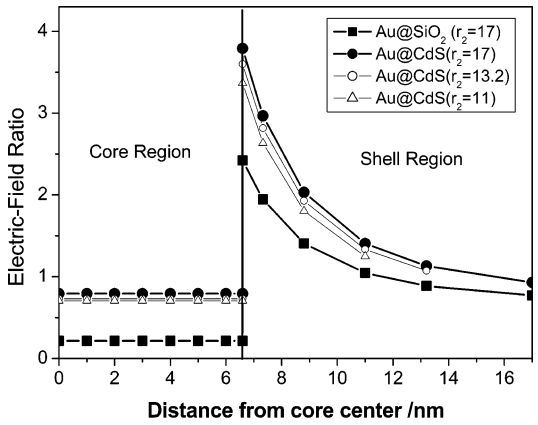

Figure 8. Spatial dependence of the electric-field ratio in different composite nanoparticles at 800 nm, functioned as the radial distance from the core center.

larger than that of the SiO_2 shell, which would result in a larger enhancement of the effective third-order nonlinear susceptibility of composite nanoparticles. Furthermore, both amplitudes of the electric field in the core and shell region increase with the increase of CdS shell thickness; however, the effective third-order nonlinear susceptibility of the Au@CdS composite film decreases due to the larger increases in the volume of the total particle.

From the above analysis for the electric field, the effective third-order nonlinear susceptibility of composite nanoparticles

can become enhanced by the core−shell structure, and can become further enhanced when the shell layer has a high refractive index and larger third-order nonlinear susceptibility $\chi_s^{(3)}$. Based on the above analysis, and considering their own nonlinear susceptibilities and refractive indices of the shell, optimization of $\chi_{eff}^{(3)}$ in a composite system with the core−shell structure can be obtained.

Conclusions

In summary, we have applied a simple route based on LBL technology to prepare 3-dimensional arrays of the Au@CdS core−shell composite nanoparticle. The CdS shell thickness is tunable by the concentration of Cd^{2+}−thiourea complexes and the film exhibits uniformly close packing structure. The 3D arrays of densely packed Au@CdS composite nanoparticles are helpful to increase the volume fraction of gold nanoparticles, and enhance the third-order nonlinear optical response. These arrays exhibit enhanced third-order optical nonlinear response and the maximum $\chi^{(3)}$ value is 1.48×10^{-9} esu. The enhancement of the third-order optical nonlinearity is dominated by localized electric field effects in the CdS shell region. Through the off-resonance femtosecond OKE experimental data and electric-field calculation for the Au@CdS film with different shell thickness and Au@SiO_2 film, the results establish the following: (a) the nonlinear optical susceptibility in the Au@CdS composite nanoparticle was enhanced due to the core−shell structure; (b) the effective third-order nonlinear susceptibility of the Au@CdS composite film decreases with the increase of the CdS shell thickness, although the amplitude of the electric field in both the core $\boldsymbol{E}_1$ and the shell $\boldsymbol{E}_2$ region increases; and (c) the electric field in the interface region between the Au core and the CdS shell get stronger enhancement compared with that between the Au core and the SiO_2 shell because CdS has a higher refractive index than SiO_2, which indicates that the further enhancement of nonlinearity could be obtained if the shell material has a higher nonlinear susceptibility and refractive indices.

Acknowledgment. Y.Y. gratefully acknowledges the Japan Society for the Promotion of Science (JSPS), Tokyo, and the NITECH 21st Century COE Program "World Ceramics Center for Environmental Harmony" for financial support. The author also thanks Mr. Ye Liu at Fudan University (PRC) for helpful calculations and discussions.

References and Notes

(1) Zhang, Z.; Kotov, N. A.; Magonov, S.; Ozturk, B. *Nature Mater.* **2003**, *2*, 413.

(2) Schneider, J. J. *Adv. Mater.* **2001**, *13*, 529.

(3) Mallik, K.; Mandal, M.; Pradhan, N.; Pal, T. *Nano Lett.* **2001**, *1*, 319.

(4) (a) Shenhar R.; Rotello, V. M. *Acc. Chem. Res.* **2003**, *36*, 549. (b) Sarathy, K. V.; Thomas, P. J.; Kulkarni, G. U.; Rao, C. N. R. *J. Phys. Chem. B* **1999**, *103*, 399.

(5) Katz, H. E. *Science* **1991**, *254*, 1485.

(6) Freeman G. R.; Grabar K. C.; Allison K. J.; Bright R. M.; Davis J. A.; Guthrie A. P.; Hommer M. B.; Jackson M. A.; Smith P. C.; Walter D. G.; Natan M. J. *Science* **1995**, *267*, 1629.

(7) Lu, Y.; Yin, Y.; Li, Z.; Xia, Y. *Nano. Lett.* **2002**, *2*, 785.

(8) Malikova, N.; Pastoriza-Santos, I.; Schierhorn, M.; Kotov, N. A.; Liz-Marzán, L. M. *Langmuir* **2002**, *18*, 3694.

(9) Neeves, A. E.; Birnboim, M. H. *J. Opt. Soc. Am. B* **1989**, *6*, 787.

(10) Yang, Y.; Nogami, M.; Shi, J. L.; Chen, H.; Liu, Y.; Qian, S. *J. Mater. Chem.* **2003**, *13*, 3026.

(11) Ando, M.; Kadono, K.; Haruta, M.; Sakaguchi, T.; Miya, M. *Nature* **1995**, *374*, 625.

(12) (a) Selvan, S. T.; Hayakawa, T.; Nogami, M.; Kobayashi, Y.; Liz-Marzán, L. M.; Hamanaka, Y.; Nakamura, A. *J. Phys. Chem. B* **2002**, *106*, 10157. (b) Liz-Marzán, L. M.; Mulvaney, P. *J. Phys. Chem. B* **2003**, *107*, 7312.

(13) Yang, Y.; Shi, J.; Chen, H.; Dai, S.; Liu, Y. *Chem. Phys. Lett.* **2003**, *370*, 1.

(14) Musick, M. D.; Keating, C. D.; Lyon, L. A.; Botsko, S. L.; Pena, D. J.; Holliway, W. D.; Mcevoy, T. M.; Richardson, J. N.; Natan, M. J. *Chem. Mater.* **2000**, *12*, 2869.

(15) Han, L.; Daniel, D. R.; Maye, M. M.; Zhong, C. *Anal. Chem.* **2001**, *73*, 4441.

(16) Ma, G. H.; He, J.; Rajiv, K.; Tang, S. H.; Yang, Y.; Nogami, M. *Appl. Phys. Lett.* **2004**, *84*, 4684.

(17) Yamaguchi, A.; Penland, R. B.; Mizushima, S.; Lane, T. J.; Curran, C.; Quaglino, J. V. *J. Am. Chem. Soc.* **1958**, *80*, 527.

(18) Bharathi, S.; Nogami, M.; Lev, O. *Langmuir* **2001**, *17*, 2602.

(19) Ung, T.; Liz-Marzán, L. M.; Mulvaney, P. *J. Phys. Chem. B* **2001**, *105*, 3441.

(20) Nanda, J.; Sapra, S.; Sarma, D. D. *Chem. Mater.* **2000**, *12*, 1018.

(21) Pankove, J. L. *Optical properties of semiconductors*; Dover Publications Inc.: New York, 1970.

(22) Liu, Y.; Li, D.; Zhu, R. Y.; You, G. J.; Qian, S. H.; Yang, Y.; Shi, J. L. *Appl. Phys. B* **2003**, *76*, 435.

(23) Krauss, T. D.; Wise, F. W. *Appl. Phys. Lett.* **1994**, *65*, 1739.

(24) Liao, H. B.; Xiao, R. F.; Fu, J. S.; Wang, H.; Wong, K. S.; Wong, G. K. L. *Opt. Lett.* **1998**, *23*, 388.

(25) Ma, G.; Sun, W.; Tang, S. H.; Zhang, H.; Shen, Z.; Qian, S. *Opt. Lett.* **2002**, *27*, 1043.

(26) Neeves, A. E.; Birnboim, M. H. *Opt. Lett.* **1988**, *13*, 1087.

(27) Debrus, S.; Lafait, J.; May, M.; Princon, N.; Prot, D.; Sella, C.; Venturini, J. *J. Appl. Phys.* **2000**, *88*, 4469.